Egyptian Journal of Chemistry

Isonicotinohydrazide Chalcone and Its Ni Complex as Corrosion Inhibitors During Acid Cleaning: Theoretical and Experimental Approaches

Adel Attia [a,*], Asmaa Aboelnaga[b], Asmaa M. Fahim[c]

[a]Electrochemistry and Corrosion Laboratory, Physical Chemistry Department, National Research Centre, Dokki, 12622 Giza, Egypt
[b]Ain Shams University, Chemistry Department, Faculty of Women of Arts, Science and Education, 11757 Heliopolis, Egypt
[c]Department of Green Chemistry, National Research Centre, Dokki, 12622 Giza, Egypt

Abstract

The reaction of isonicotinohydrazide (**1**) with [1]H-indole-3-carbaldehyde (**2**) to produce the corresponding (Z)-N'-((1H-indol-3-yl)methylene) isonicotinohydrazide (**Ch**) was investigated. A novel Ni complex was synthesized from this chalcone (**ChN**). These compounds were theoretically studied. A maximum inhibition efficiency of 82.4% and 73.5% for the **Ch** and **ChN** inhibitors respectively from weight loss while it was ~86.9% and ~92.3% for the **Ch** and **ChN** inhibitors respectively from potentiodynamic polarization. The polarization resistance for the **ChN** inhibitor was higher than that for the **Ch** inhibitor and concomitant decrease in the corrosion rate with increasing the **ChN** inhibitor concentration was observed. The K_{ads} was 11.4824 M^{-1} and 6.8667 M^{-1} for **Ch** and **ChN** inhibitors respectively. The free energy of adsorption ($\Delta G^o_{ads.}$) was found to be -12.1685 kJ mol^{-1} for the **Ch** inhibitor and -14.7326 kJ mol^{-1} for the **ChN** inhibitor. This indicates that both the **Ch** and **ChN** inhibitors were physically adsorbed onto the surface of the mild steel, with the **ChN** being preferentially adsorbed. Raman spectroscopy analysis of the mild steel reveals the presence of γ-FeOOH on its surface while additional peaks were detected after the addition of the **Ch** and **ChN** inhibitors associated with the adsorption of these inhibitors.

Keywords: Isonicotinohydrazide Chalcone; Schiff base; Ni-complex; computational studies, corrosion inhibition

1. Introduction

Acid contact with steel can occur during various industrial processes for a variety of reasons. For example, in drilling work to explore water, gas and oil processes to overcome the obstacles, such as rocks at production sites, acidic solutions can be pumped into boreholes through an acidification technique.

Hydrochloric acid is commonly used during acidification to facilitate the drilling process in carbonate rock (e.g. limestone or dolomite) to reach the water, oil or gas wells. On the other hand, the pipes used to pump the acid are made of steel, which as the wall of the wells is easily corroded by the hydrochloric acid attack.

Boilers, heat exchangers and oil and gas tanks are mainly made of steel structures due to their strength and low cost. From time to time these corroded structures require acidification after service and are therefore exposed to the acid. During these processes, the steel can lose its strength and the process may need to be shut down, which is time consuming and costs the decision maker a fortune. For this reason, finding an ideal inhibitor to use during these industrial processes is crucial to reduce

the aggressiveness of the HCl used during pickling or cleaning to remove unwanted rust or scale.

Organic compounds are those of continuous hydrocarbons and contain heteroatoms as polar atoms, such as O, P, N and S, which are widely used as inhibitors, these heteroatoms aiding in the adsorption of these compounds onto the metal surface through physiosorption or chemisorption processes. This consequently isolates the metal surface from the aggressive ions in the solution and blocks the active site on the metal/alloy surface, thus reducing the corrosion rate (CR) [1-3].

These organic inhibitors were widely used to protect ferrous and non-ferrous metals [4-7], but in the above-mentioned processes, mild steel (MS) was heavily used for the material's feasibility, such as its cost, strength, and wide range of industrial applications.

The isonicotinohydrazidechalcone derivatives presented in this study have already been characterized in the literature, and their antibacterial, anticancer and anti-inflammatory effects have been investigated [8]. However, previous studies did not examine their metal complexes as corrosion inhibitors, which, to the best of the authors' knowledge, is the first time that they have been synthesized as a corrosion inhibitor during acid cleaning.

The aim of this work is to investigate isonicotinohydrazideChalcone derivative and its Ni complex as corrosion inhibitors during acid cleaning of MS in 0.5 M HCl by some experimental and theoretical approaches.

2. Experimental

2.1. Instrumentation

All melting points were measured on a Gallenkamp melting point apparatus and were uncorrected. Infrared spectra were recorded in potassium bromide discs on a PyeUnicam SP-3-300 and a Shimadzu FT-IR 8101 PC infrared spectrophotometer. NMR spectra were recorded on a Varian Mercury VX-300 NMR spectrometer. ^{1}H NMR spectra were recorded at 300 MHz in dimethyl sulfoxide (DMSO-d6). ^{1}H NMR spectra were

recorded at 300 MHz in dimethyl sulfoxide (DMSO-d6).

2.2. Materials and methods

Isonicotinohydrazide, 1H-indole-3-carbaldehyde, acetic acid and $NiCl_2 \cdot 6H_2O$, were purchased from Aldrich Chemical CO.

2.2.1 Synthesis of (Z)-N'-((1H-indol-3-yl)methylene)isonicotinohydrazide (3) (Z)-N'-((1H-indol-3-yl)methylene)isonicotinohydrazide (**Ch**).

Ethanol solution of isonicotinohydrazide (1) (1.37 g, 0.01 mol) with 1H-indole-3-carbaldehyde (2) (1.44g, 0.01 mol) was added to a of few drops of ACOH, for 4 hours heated to reflux, then monitored by TLC to know that the reaction was complete, upon completion of the reaction the product was separated as a yellow colored amorphous product which was filtered, dried, and recrystallized from ethanol to give (Z)-N'-((1H-indol-3-yl)methylene)isonicotinohydrazide(**Ch**): (Yield: 80%;) mp 188-200°C, Rf = 0.38 (1:2 EtOAc-petroleum ether); IR (KBr) cm−1: 3155 (NH), 1618 (C=N),1677(CO), 1575 (NH bend), 1245 (C-N); ^{1}H NMR (300 MHz, DMSO-d6) δ 11.73 (s, 1H,NH-indole), 9.98 (s, 1H, N=CH), 8.87(d, J = 5.48 Hz, 1H,N = CH, pyridine), 8.77(dd, J = 7.48 Hz, 1H, pyridine), 8.64 (d, 1H, J = 7.48 Hz, pyridine), 8.31-7.15(m, 7H, Ar-H). Mass spectra (M±) m/z = 264.28 Anal. Calcd for $C_{15}H_{15}N_4O$: C, 68.17; H, 4.58; N, 21.20. Found: C, 68.33; H, 4.52; N, 21.09%.

2.2.2 Synthesis of metal Ni-complex

Hot ethanolic solution of compound **Ch** (0.264, 1 mmol) (60°C) was treated with ethanolic $NiCl_2 \cdot 6H_2O$ (1 mmol) (60°C) in a mixture of EtOH/DMF (15 mL, 7:3 v/v). The obtained mixture was refluxed for 6 h and the solvent was dispersed under pressure to give the precipitates which were washed many times with EtOH and the yield calculated.

$C_{15}H_{15}N_4NiO_4$: red solid, in 75% yield, m.p=>300 °C, anal found/(calculated) (357.05), C, (50.32) 50.35%; H, (4.22)4.25%, N, (15.65) 15.68%, Ni, (16.39) 16.42%; IR (KBr) νmax/cm−1: v̄=3415 (NH) indole, 1616 (C-O), 1358 (Ni-N), 3044 (CH-aromatic), 459 (Ni-O), ^{1}H NMR (300 MHz, DMSO-d6) δ= 11.74 (s, 1H,NH-indole), 9.83(s, 1H, CH, indole), 8.76 (d, 2H, pyridine), 7.751 (d, 2H.CH), 7.4 (m, 4H, CH aromatic), 7.17

_____

(s, 1H, CH), 4.97 (S, 3H, OH D_2O-exchangable). Mass spectra (M±) m/z = 355.

2.3. Corrosion study
2.3.1. Gravimetric method

MS was used as the working electrode throughout the weight loss technique. The electrolyte solution was 0.5 M HCl which was reported early on to be used in acid cleaning [9-12]. In the weight loss technique, we used 250 mL of 0.5M HCl, in which the steel coupons were suspended by plastic wire so that they were completely immersed freely in the HCl in a closed glass container, and the weight for these steel coupons was taken before and after certain times. The temperature was thermostated at 30°C with accuracy of 1°C.

The CR calculated from weight loss technique was determined from Eq. 1

$$Corrosion\,rate\,(mpy) = \frac{3445.15W}{DAT} \quad (1)$$

Where W is the weight loss in grams; A is the total area of the specimen in cm^2, T is the corrosion time in hours and D is the density of the specimen in $g.cm^{-3}$; of 7.85 $g.cm^{-3}$ for MS.

Two corrosion inhibitors (Chalcone compounds) defined as **Ch** and **ChN** (see Fig. 1), Eq. (1) shown above was used to calculate the CR after the addition of these two inhibitors and therefore rate their CR. On the other hand, the surface coverage (θ) and the inhibition efficiency (IE%) were calculated from Eq. 2 and 3 shown below respectively, where W_o represents the weight of the samples before immersion.

Inhibitor (I): **Ch**   Inhibitor (II): **ChN**
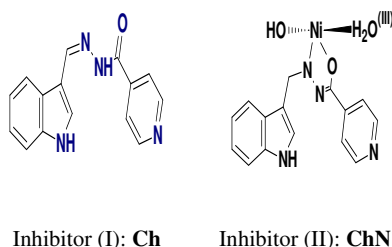
Fig. 1 The proposed structure of the used inhibitors in this work

$$\theta = \frac{W}{W_o} \quad (2)$$

$$IE(\%) = \frac{W}{W_o} \times 100 \quad (3)$$

2.3.2. Open Circuit Potential

The electrodes were left in 0.5 M HCl and after the addition of inhibitors the potential was recorded. In this technique the potential was always measured against a saturated calomel electrode reference electrode (SCE).

2.3.3. Potentiostatic polarization (PDP)

MS electrodes were used in a 3-electrode cell, in which Pt wire was used as the counter electrode and SCE as the reference electrode. The scan rate used throughout the experiments was 1 mV/s and the potentiostat used was a PS6 potentiostat-galvanostat system from Meinsberger (Germany). The temperature was thermostated at 30°C with accuracy of 1°C.

2.3.4. Raman Spectroscopy

The Raman shift of the MS surface after its immersion in 0.5 M HCl and after the addition of **Ch** and **ChN** inhibitors were measured on an i-Raman Plus 532S portable laser Raman spectrometer (laser wavelength is 532 nm as excitation source, laser power is 30 mW, and the spectral resolution was <4.5 cm^{-1}) performed with BAC151C Raman Video Micro-Sampling System (B&W TEK, USA), and 20-100X objectives.

3. Results and discussion

3.1. Organic synthesis of inhibitors

The condensation reaction between isonicotinohydrazide (1) with 1H-indole-3-carbaldehyde (2) in a mixture of EtOH/acetic acid and the obtained (Z)-N'-((1H-indol-3-yl)methylene)isonicotinohydrazide (3) in excellent yield which was confirmed by spectral analysis such as FT-IR (see Fig. 2). FT-IR showed that the presence of an NH group at about 3543 cm^{-1} for the **Ch** inhibitor and the absence of this band in the FTIR of the **ChN** inhibitor indicated that Ni metal make chelation with the NH of **Ch** and decreases the intensity of NH in this region due to formation of N-N. Furthermore, the presence of a shoulder for the **ChN** inhibitor near 3450 cm^{-1} indicated the absence of an N-H group [13]

_____
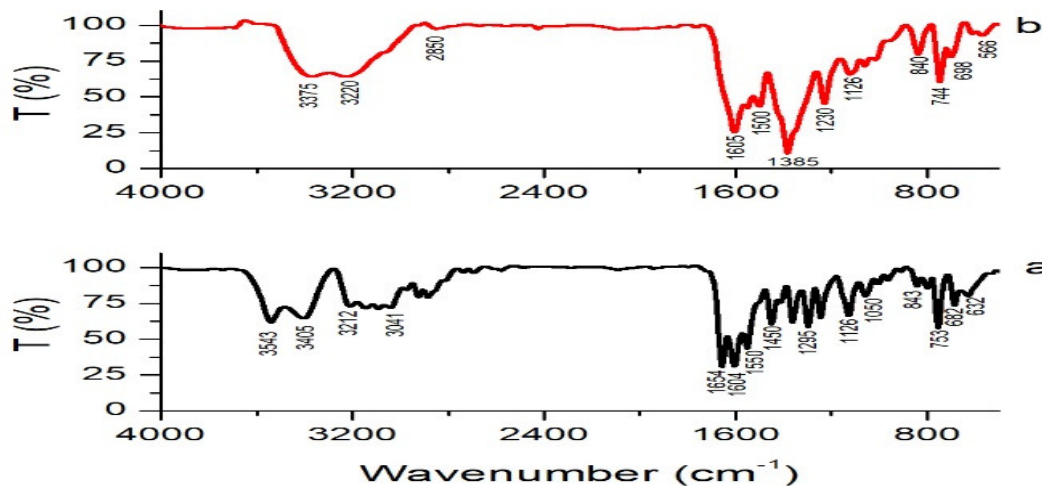
Fig. 2 FITR of the synthesized **Ch** (a) and **ChN** (b)

For the **Ch** inhibitor, the characteristic C=O band appeared at 1654 cm^{-1}, which was attributed to the presence of the primary amide group. This characteristic band disappeared in the **ChN** inhibitor (the Ni complex) and was replaced by a C-O bond.

The C-O stretching was reported to be in the region of 1300-1000 cm^{-1}[13], however, the presence of the Ni bounded to the oxygen shifted this band up to where it is assigned to the C-O stretching which appears at 1385 cm^{-1} which has a Ni in the nearby.
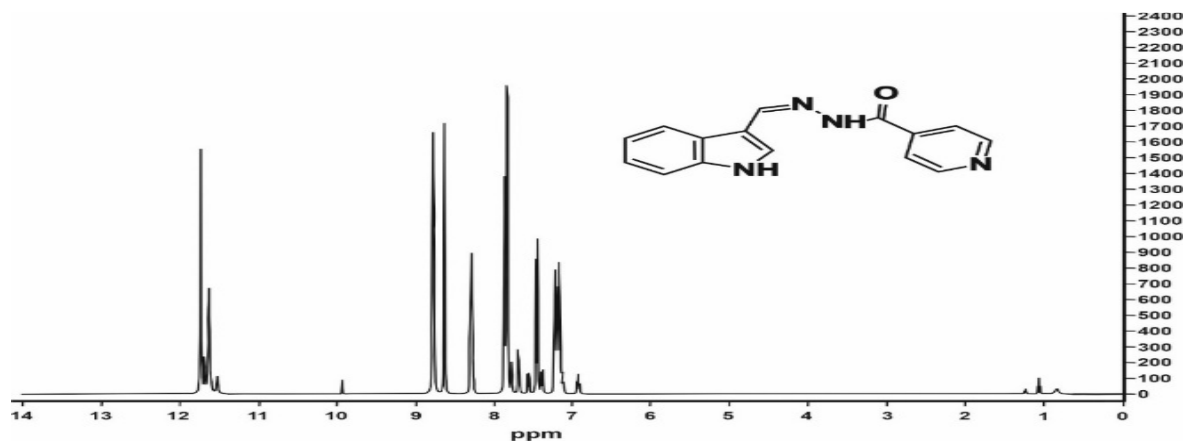
Fig. 3 ^{1}H NMR of the synthesized **Ch** compound

Figures 3 and 4 show the ^{1}H NMR of this chalcone revealing the presence of the N=CH signal from azomethine protons as singlets at 9.98 ppm (see Fig. 3) and NH of the indole signal as singlets at 11.78 ppm (see Fig. 4).

Reactivity of the ethanolic solution of the isonicotinohydrazide derivative ligand (**Ch**) with

NiCl$_2$.6H$_2$O in of 1:1 (metal:ligand) ratio. The newly synthesized Ni chelate complex in this work was stable at 27°C and soluble in DMF and DMSO as displayed in Scheme 1. The spectral characterization, elemental analysis and the molecular formula was determined to C$_{15}$H$_{15}$N$_4$NiO$_3$ and its melting point >300°C.

_____

_____
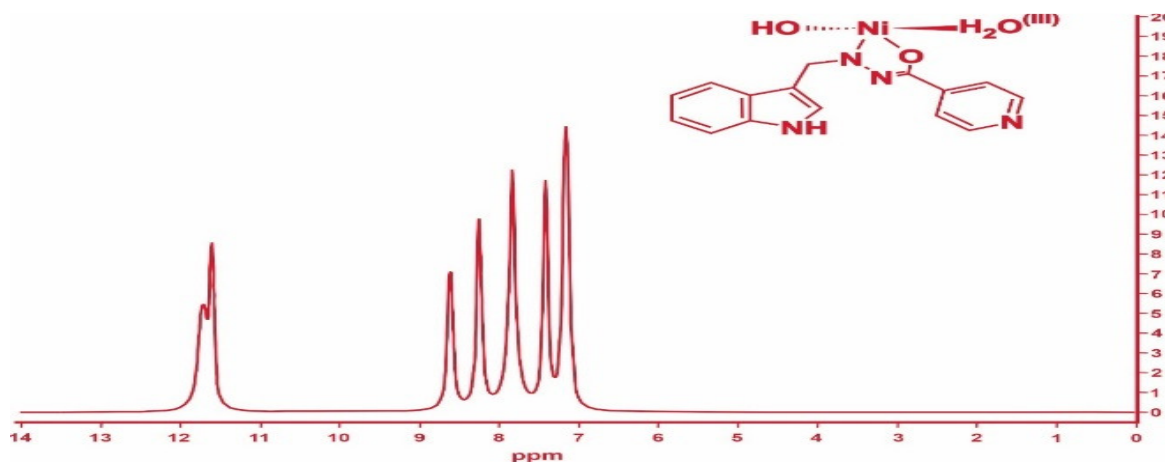
Fig. 4 ^{1}H NMR of the synthesized **ChN** compound

The two structures of the inhibitors (Chalcone and its Ni-complex) were shown in Fig. 1

3.2. Theoretical investigation

3.2.1. Geometric Optimization and Characterization of Chalcone and Ni-Chalcone complex

The DFT studies are quite significant to realize additional knowledge on the corrosion inhibition phenomenon. The corrosion inhibition effectiveness of a molecule as corrosion inhibitor correlates with some quantum parameters (E_{HOMO}, E_{LUMO}, ΔE (band gap energy), η (absolute hardness), σ (absolute softness), χ (electronegativities), and ΔN (electronic charge) and Mulliken charges) according to Eq. 5-8 [14-17] shown below. The studied quantum factors can be observed by optimizing the studied inhibitor [18, 19]. In this study we optimized the chalcone **Ch** and Ni complex to know their energies and physical characterization as shown in Table 1 and Fig. 5 (A,B) using the DFT/B3PW91/LANL2DZ basis set and we found that the (Z)-N'-((1H-indol-3-yl)methylene)isonicotinohydrazide (**Ch**) had an energy − (−23293.259 eV) (−537155.18356 kcal/mole) and has π-effect properties resulting from the presence of different substituents in pyridine and indole rings relative to each other. Furthermore, Frontier Molecular Orbitals Theory (FMO's) states that the chemical reactivity of a molecule mainly depends on an optimized geometry structure and electron density distribution in HOMO and LUMO energy gap and the energy gap in compound (**Ch**) showed $\Delta E=10.22748$ eV and this high energy gap in this chalcone related to high reactivity due to the presence of NH group acting as a chelating center and confirmed this reactivity in

metal complexation with NiCl$_2$.6H$_2$O and also the optimization of this complex where we found that the energy of this complex becomes lower than chalcone and yield energy (−32486.60081 eV) (−749158.6206 kcal/mol) and energy gap between HOMO-LUMO was $\Delta E=2.488228$ eV. The polarity of charge separation of Ch showed more dipole moment than **ChN** with difference between them 0.2701D which meant that **ChN** is a Ni complex.

In addition, the chemical potential (Pi) value of the Ni complex was negative, while the electrophilicity index (χ) showed a positive charge. This observation showed that the Ni-complex was a good donor of electrons [20]. Also, the molecular electrostatic potential, at which the nuclei and electrons of a molecule generate the surrounding space proven to be a very useful analytical tool in the study of molecular reactivity, including recognition interactions [21].
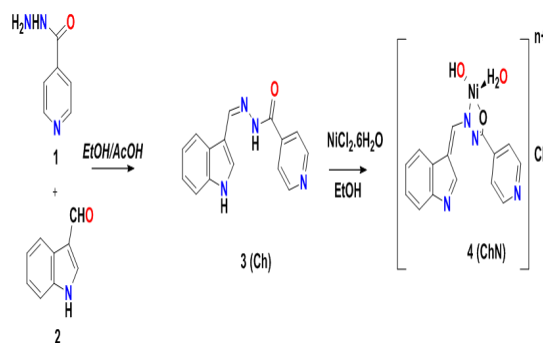
Scheme 1 Chelation of nickel chloride with isonicotinohydrazide derivative ligand.

_____

Thus, the chalcone (**Ch**) and Ni complex (**ChN**) mark a specific point that indicates that there is a uniform distribution of surface contour for these rings rather than the other Ni complex since they contain the bound NH, C=O contained between indole and pyridine rings acting as electrophilic centers which induced more protonation and gave more reactivity and interaction [21] as shown in Fig. 5 (A, B).

$$\Delta E = E_{LUMO} - E_{HOMO} \quad (1) \qquad Pi = -\chi \quad (5)$$

$$\chi = \frac{-(E_{HOMO} + E_{LUMO})}{2} \quad (2) \qquad S = \frac{1}{2}\eta \quad (6)$$

$$\eta = \frac{(E_{LUMO} - E_{HOMO})}{2} \quad (3) \qquad \omega = \frac{Pi^2}{2} \quad (7)$$

$$\sigma = \frac{1}{\eta} \quad (4) \qquad \Delta N_{max} = -\frac{Pi}{\eta} \quad (8)$$

Furthermore, we optimized the chalcone (**Ch**) and its Ni complex (**ChN**) with steel to know their inhibition activity on the steel surface, and we noticed that geometrically optimized structure of chalcones and Ni complex inhibitors have planar orientation. Therefore, it will not adsorb in a flat orientation on the MS surfaces. The reactivity of steel-surfaced chalcone with energy (−27081.4101 eV) (−624511.995 kcal/mol) and the HOMO of the inhibitor showed that the electron density is distributed only over the Fe atom and LUMO appreciable **electron density over the Fe part of the molecule and with energy** gap ΔE= 0.004 eV with the lowest value and did not accumulate completely on the steel surface.

Table 1 Ground state energies of compounds Chalcone, and its Ni complex and their association with Fe steel utilizing DFT/B3PW91/ LANL2DZ basis set with their physical parameters

DFT/ B3PW91/LANL2DZ							
Physical parameters	*Chlcone*		*Chalcone with Fe steel*		*Compound Ni complex*		*Ni complex with Fe steel*
E_T (eV)	-23293.259		-27081.410		-32486.601		-35844.003
E_{HOMO} (eV)	-4.959		-5.415		-5.395		-4.829
E_{LUMO} (eV)	5.268		-5.411		-2.906		-4.742
E_g (eV)	10.227		0.004		2.488		0.087
μ (D)	5.9108		4.876		6.1809		3.546
χ (eV)	-0.154		5.413		4.151		4.785
η (eV)	5.114		0.002		1.244		0.004
σ (eV)	0.196		524.990		0.804		22.968
P_i (eV)	0.154		-5.413		-4.151		-4.785
S (eV)	0.098		*262.495*		*0.402*		11.484
ω (eV)	0.002		7690.937		6.923		262.987
ΔN_{max}	−0.030		2706.5		3.337		1196.250
Mulliken atomic charge	N_{10}	−0.133	N_{10}	−0.403	N_{10}	−0.585	N_{10}	−0.780
	N_9	−0.469	N_9	−0.966	N_9	−0.137	N_9	−0.590
	C_1	0.254	C_1	0.832	C_1	0.049	O_8	−0.804
	O_8	−0.244	O_9	−0.934	O_8	−0.275	Ni_{21}	5.783
	H_{25}	0.303	Fe_{33}	1.2929	Ni_{21}	0.387	Fe_{39}	−2.864
[a] $E_g = E_{LUMO} - E_{HOMO}$.							

_____

(A)

(B)

(C)

(D)
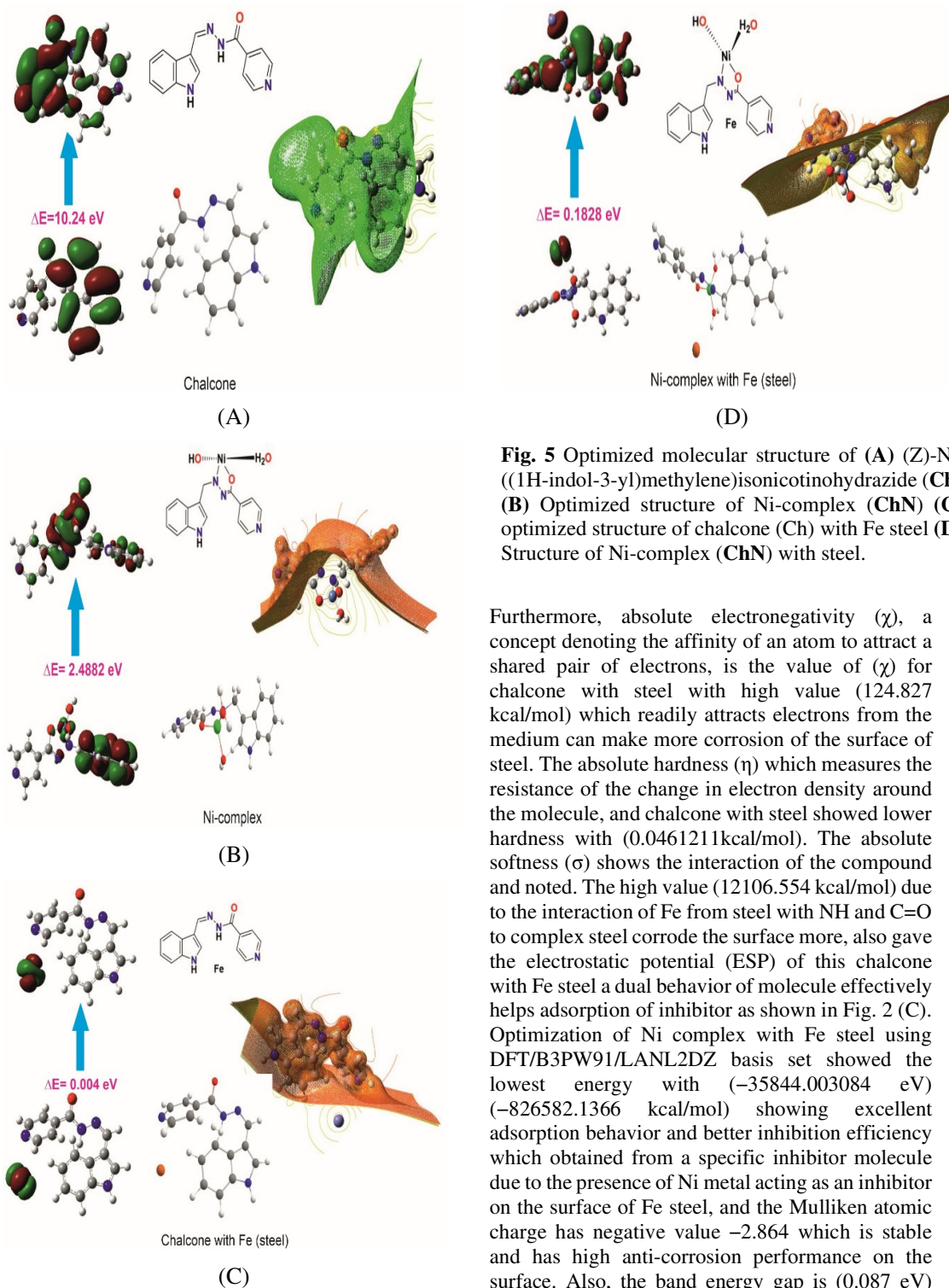
Fig. 5 Optimized molecular structure of **(A)** (Z)-N'-((1H-indol-3-yl)methylene)isonicotinohydrazide (**Ch**) **(B)** Optimized structure of Ni-complex (**ChN**) **(C)** optimized structure of chalcone (Ch) with Fe steel **(D)** Structure of Ni-complex (**ChN**) with steel.

Furthermore, absolute electronegativity (χ), a concept denoting the affinity of an atom to attract a shared pair of electrons, is the value of (χ) for chalcone with steel with high value (124.827 kcal/mol) which readily attracts electrons from the medium can make more corrosion of the surface of steel. The absolute hardness (η) which measures the resistance of the change in electron density around the molecule, and chalcone with steel showed lower hardness with (0.0461211kcal/mol). The absolute softness (σ) shows the interaction of the compound and noted. The high value (12106.554 kcal/mol) due to the interaction of Fe from steel with NH and C=O to complex steel corrode the surface more, also gave the electrostatic potential (ESP) of this chalcone with Fe steel a dual behavior of molecule effectively helps adsorption of inhibitor as shown in Fig. 2 (C). Optimization of Ni complex with Fe steel using DFT/B3PW91/LANL2DZ basis set showed the lowest energy with (−35844.003084 eV) (−826582.1366 kcal/mol) showing excellent adsorption behavior and better inhibition efficiency which obtained from a specific inhibitor molecule due to the presence of Ni metal acting as an inhibitor on the surface of Fe steel, and the Mulliken atomic charge has negative value −2.864 which is stable and has high anti-corrosion performance on the surface. Also, the band energy gap is (0.087 eV) which improved anti-corrosion behavior and stability with Ni with Fe steel and the ESP behavior of Fe and Ni with all positive and negative charges and not widely attached like chalcones but in all

_____

molecule, confers and gave it more stability which reaffirms the experimental results as will be discussed later.

3.3. *Experimental Corrosion study*

3.3.1. *Gravimetric results*
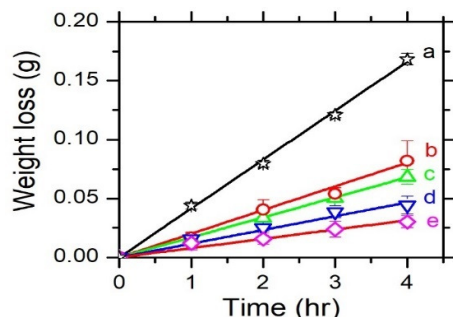
Fig. 6 Weight loss of mild steel in 0.5 M HCl at 30°C in presence of different concentrations of **Ch** inhibitor of 0 ppm (a), 25 ppm (b), 50 ppm (c), 75 ppm (d) and 100 ppm (e).
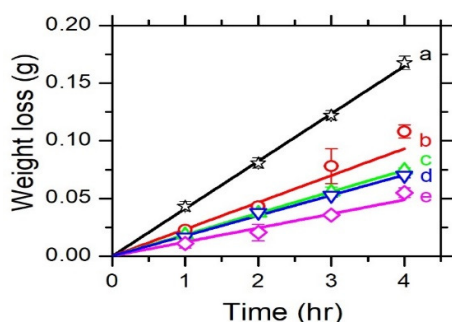
Fig. 7 Weight loss of mild steel in 0.5 M HCl at 30 °C in presence of different concentrations of **ChN** inhibitor of 0 ppm (a), 25 ppm (b), 50 ppm (c), 75 ppm (d) and 100 ppm (e).

The weight loss of MS in the presence of Ch and **ChN** inhibitors is shown in Figs. 6 and 7.

The inhibition during acid cleaning was apparently increased by both **Ch** and **ChN** compared to the control (curve a) as shown in Figs 6 and 7.

The weight loss results show that **Ch** inhibition was better than **ChN**. The surface coverage (θ), inhibition efficiency (IE, %), and CR (mpy) were calculated and tabulated in Tables 2 and 3.

3.3.2. *Open-Circuit Potential (OCP)*
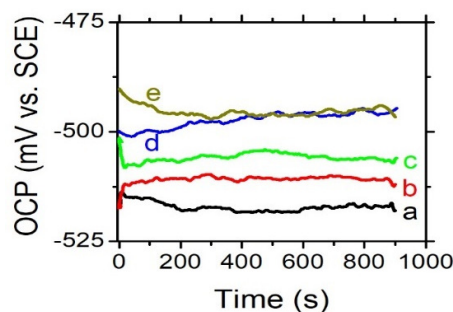
Fig. 8 OCP of mild steel in 0.5M HCl at 30°C in presence of different concentrations of **Ch** inhibitor 0 ppm (a), 25 ppm (b), 50 ppm (c), 75 ppm (d), 100 ppm (e).

The OCP of both **Ch** and **ChN** inhibitors showed inhibition of MS during acid cleaning. From Figs 8 and 9, both **Ch** and **ChN** showed a shift in the OCP in the noble direction compared to the control (no addition of inhibitor). This shift in the noble direction was observed for both **Ch** and **ChN** inhibitors suggested that both selected inhibitors are suitable for this inhibition.

The OCP could not provide information about the CR, however the polarization data and weight loss provided this information. The relatively high noise to signal ratio observed for the **Ch** inhibitor at
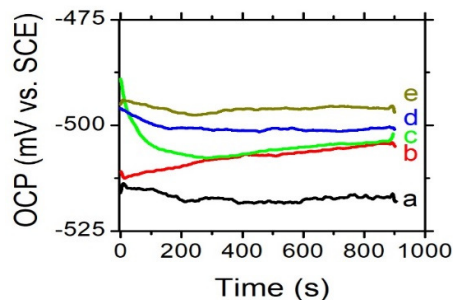
Fig. 9 OCP of mild steel in 0.5M HCl at 30°C in presence of different concentrations of ChN inhibitor 0 ppm (a), 25 ppm (b), 50 ppm (c), 75 ppm (d), 100 ppm (e).

concentration of 75 and 100 ppm (Fig. 8, curves d and e respectively) may indicate that this inhibitor involve a roughened surface or some localized corrosion. This noise was reduced using the same concentrations of **ChN** inhibitor (Fig. 9, curves d and e respectively).

Table 2 Weight loss of Ch inhibitor during acid cleaning of mild steel in 0.5 M HCl at 30 °C

Concentration (ppm)	Cleaning time (hr)	Θ	IE (%)	CR (mpy)
0	1	NA	NA	0
	2	NA	NA	1.936
	3	NA	NA	1.75078
	4	NA	NA	1.77724
25	1	0.6514 (±0.1049)	65.1449 (±10.4942)	0.73794
	2	0.5491 (±0.0259)	54.9096 (±2.5936)	0.89377
	3	0.5572 (±0.0485)	55.7235 (±4.8541)	0.79331
	4	0.5932 (±0.0441)	59.3240 (±4.4093)	0.90406
50	1	0.6663 (±0.0569)	66.6304 (±5.6876)	0.67694
	2	0.5685 (±0.0073)	56.8475 (±0.7309)	0.73647
	3	0.5777 (±0.0071)	57.7666 (±0.7124)	0.73941
	4	0.6023 (±0.0367)	60.2273 (±3.6674)	0.75246
75	1	0.7761 (±0.1445)	77.6087 (±14.4496)	0.68796
	2	0.7402 (±0.0584)	74.0245 (±5.8377)	0.55236
	3	0.7356 (±0.0417)	73.5642 (±4.1738)	0.56816
	4	0.7499 (±0.0323)	74.9866 (±3.2338)	0.48841
100	1	0.7380 (±0.1276)	73.8043 (±12.7587)	0.34839
	2	0.7978 (±0.0612)	79.7804 (±12.7587)	0.41895
	3	0.7997 (±0.0564)	79.9748 (±5.6402)	0.28077
	4	0.8246 (±0.0297)	82.4592 (±2.9669)	0.37154

3.3.3. Potentiodynamic polarization
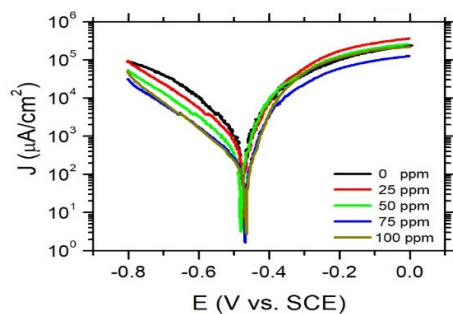
Fig. 10 Potentiodynamic polarization of mild steel in 0.5M HCl at 30°C in presence of different concentrations of **Ch** inhibitor of 0 ppm (a), 25 ppm (b), 50 ppm (c), 75 ppm (d) and 100 ppm (e).
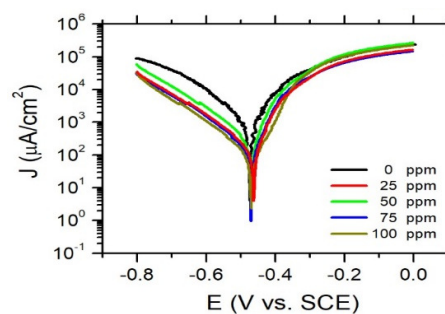
Fig. 11 Potentiodynamic polarization of mild steel in 0.5M HCl at 30°C in presence of different concentrations of **ChN** inhibitor of 0 ppm (a), 25 ppm (b), 50 ppm (c), 75 ppm (d) and 100 ppm (e).

A. Attia et. al.

Table 3 Weight loss of **ChN** inhibitor during acid cleaning of mild steel in 0.5 M HCl at 30 °C

Concentration (ppm)	Time of cleaning (hr)	Θ	IE%	CR (mpy)
0	1	NA	NA	0
	2	NA	NA	1.936
	3	NA	NA	1.75078
	4	NA	NA	1.77724
25	1	0.5065 (±0.0154)	50.6522 (±1.5372)	1.00108
	2	0.4438 (±0.0375)	44.3798 (±3.7457)	0.94926
	3	0.3451 (±0.1258)	34.5088 (±12.5866)	1.14661
	4	0.3700 (±0.0321)	37.0047 (±3.2141)	1.19181
50	1	0.6087 (±0.0922)	60.8696 (±9.2231)	0.7938
	2	0.5233 (±0.0475)	52.3256 (±4.7506)	0.81365
	3	0.5323 (±0.0368)	53.2326 (±3.6810)	0.81879
	4	0.5714 (±0.0202)	57.1387 (±2.01913)	0.81089
75	1	0.6043 (±0.0953)	60.4348 (±9.53057)	0.72986
	2	0.5375 (±0.0658)	53.7468 (±6.5777)	0.83129
	3	0.5688 (±0.0267)	56.8850 (±2.6717)	0.77322
	4	0.5813 (±0.0276)	58.1294 (±2.76085)	0.7712
100	1	0.7348 (±0.1230)	73.4783 (±12.2975)	0.53802
	2	0.7274 (±0.1041)	72.7390 (±10.4147)	0.46526
	3	0.6784 (±0.0475)	67.8421 (±4.7497)	0.56301
	4	0.6865 (±0.0346)	68.6480 (±3.4614)	0.59315

_____
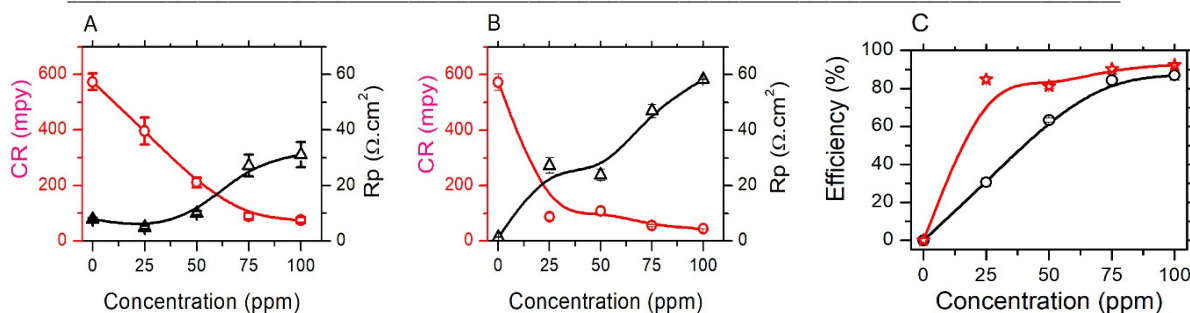
Fig. 12 Corrosion rate and polarization reisstance vs amount of inhibitor added of **Ch** (A) and **ChN** (B) and their inhibition efficincy on mild steel in 0.5M HCl upon amount added (cicrcl: **Ch** inhibitor while star: **ChN** inhibitor) (C).

The CR was determined according to Eq.9

$$CR = 0.129 \left(\frac{I_{corr} . EW}{D} \right) \qquad (9)$$

CR in mpy, EW is equivalent weight of MS, D is density of the MS, I_{corr} is corrosion current in $\mu A.cm^{-2}$ obtained from PDP, and inhibition efficiency was determined using Eq. (10).

Tables 4 and 5 show the corrosion parameters of **Ch** and **ChN** inhibitors such as corrosion potential (E_{corr}), Tafel cathodic slope (β_c), Tafel anodic slope (β_a), and corrosion current density (I_{corr}) calculated from PDP data by extrapolation of the Tafel line.

Using Eq. 10, the corrosion inhibition efficiency (IE, %) of **Ch** and **ChN** inhibitors was calculated.

.

$$IE(\%) = \frac{I_{corr} - I_{corr(inh)}}{I_{corr}} \times 100 \qquad (10)$$

Using a concentration of 100 ppm of **Ch** inhibitor, the maximum inhibition efficiency obtained was about 87% while the CR was about 75 mpy (see Table 4). On the other hand, using a concentration of 100 ppm of **ChN** inhibitor, the maximum inhibition efficiency obtained was about 92% while the CR was about 44 mpy (see Table 5).

The polarization resistance (R_p) was calculated using the Stern-Geary equation[22] as indicated in Eq. 11 and their values at various concentrations of **Ch** and **ChN** inhibitors are tabulated in Tables 4 and 5.

$$R_p = \frac{\beta_a \times \beta_c}{2.303 \times I_{corr} \times (\beta_a + \beta_c)} \qquad (11)$$

The CR rapidly decreased until the concentration of **Ch** inhibitor reached 75 ppm as shown in Fig. (12A). Beyond this concentration, the CR had almost reached steady state. This was in contrast to the CR of the **ChN** inhibitor (Fig. (12B)), where the CR dropped sharply at 25 ppm before steadily declining. The polarization resistance increased for both inhibitors with increasing inhibitor concentration; however, it was about 58 ohm.cm² for the **ChN** inhibitor compared to about 31 ohm.cm² for the **Ch** inhibitor.

The inhibition efficiency of both inhibitors, **Ch** and **ChN**, was shown in Fig. (12C) in different concentration ranges ranging from 0-100 ppm. The **ChN** inhibitor had higher efficiency than the **Ch** inhibitor. The inhibition efficiency of the **ChN** inhibitor was about 85% at 25 ppm and reached about 92% at 100 ppm, whereas it was about 30% at 25 ppm and reached about 87% at 100 ppm. This showed that **ChN** was far superior to **Ch** inhibitor in terms of cost when used at low concentrations.

The most efficient CR obtained was at the highest polarization resistance. This can be explained on the basis of the surface coverage (θ) of adsorbed molecules. With complete surface coverage, this is the lowest CR as this is ideally the case and the adsorbed molecules will block the active sites on the surface of the steel and consequently isolate the steel from the corrosive media. The surface coverage can be influenced by the type [23-26] and concentration of inhibitors [5, 27, 28].

The surface coverage can be obtained directly from the PDP from the corrosion current of the inhibited and uninhibited samples [29-31].

$$\theta = \frac{I_{corr} - I_{corr(inh)}}{I_{corr}} \qquad (12)$$

Table 4 Corrosion parameters for mild steel in 0.5 M HCl in the presence of different concentrations of the **Ch** inhibitor at 30°C.

Conc. (ppm)	$-E_{corr}$ (V)	I_{corr} ($\mu A/cm^2$)	$-\beta c$ (V/decade)	βa (V/decade)	CR (mpy)	Rp (ohm.cm^2)	IE (%)
0	0.477 (± 0)	1246.028 (± 64.376)	0.007 ($\pm 2.404 \times 10^{-4}$)	0.011 ($\pm 5.727 \times 10^{-4}$)	573.332 (± 29.621)	7.833 (± 0.405)	0
25	0.469 ($\pm 5.6 \times 10^{-4}$)	860.995 (± 106.531)	0.006 ($\pm 7.071 \times 10^{-5}$)	0.016 (± 0.003)	396.167 (± 49.018)	4.883 (± 0.604)	30.587 (± 12.136)
50	0.480 (± 0.002)	458.205 (± 37.851)	0.006 ($\pm 3.54 \times 10^{-4}$)	0.017 (± 0.001)	210.832 (± 17.416)	10.040 (± 0.829)	63.256 (± 1.139)
75	0.469 (± 0.001)	194.082 (± 27.991)	0.007 ($\pm 3.535 \times 10^{-5}$)	0.017 ($\pm 2.970 \times 10^{-4}$)	89.302 (± 12.879)	27.192 (± 3.922)	84.345 (± 3.055)
100	0.466 (± 0.003)	162.852 (± 23.487)	0.007 ($\pm 1.909 \times 10^{-4}$)	0.021 (± 0.001)	74.933 (± 10.807)	31.140 (± 4.491)	86.864 (± 2.564)

Table 5 Corrosion parameters for mild steel in 0.5 M HCl in the presence of different concentrations of the **ChN** inhibitor at 30°C.

Conc. (ppm)	$-E_{corr}$ (V)	I_{corr} ($\mu A/cm^2$)	$-\beta c$ (V/decade)	βa (V/decade)	CR (mpy)	R_p (ohm.cm^2)	IE (%)
0	0.477 (± 0)	1246.028 (± 64.376)	0.007 ($\pm 2.40 \times 10^{-4}$)	0.011 ($\pm 5.73 \times 10^{-4}$)	573.332 (± 29.621)	1.368 (± 0.050)	0
25	0.462 ($\pm 2.83 \times 10^{-4}$)	190.567 (± 27.484)	0.007 ($\pm 6.29 \times 10^{-4}$)	0.019 ($\pm 2.26 \times 10^{-4}$)	87.685 (± 12.646)	27.229 (± 2.791)	84.743 (± 1.417)
50	0.469 (± 0.001)	235.476 (± 28.331)	0.008 ($\pm 9.12 \times 10^{-4}$)	0.021 ($\pm 7.07 \times 10^{-6}$)	108.349 (± 13.036)	23.829 (± 2.035)	81.135 (± 1.299)
75	0.469 (± 0.001)	120.795 (± 8.733)	0.008 ($\pm 4.17 \times 10^{-4}$)	0.021 (± 0.001)	55.581 (± 4.018)	46.921 (± 2.402)	90.274 (± 1.203)
100	0.468 ($\pm 2.98 \times 10^{-4}$)	95.419 (± 0.575)	0.008 ($\pm 7.78 \times 10^{-5}$)	0.021 (± 0.030)	43.905 (± 0.265)	58.394 (± 0.249)	92.333 (± 0.350)

The inhibition efficiency shown in Tables 4 and 5 correlates to surface coverage by the following relationship:

$$EI(\%) = \theta \times 100\% \qquad (13)$$

The **Ch** and **ChN** inhibitors in 0.5 M HCl as the aggressive environment probably adsorb at the MS/hydrochloric acid solution interface, this adsorption process being dependent on the type of electronic properties of the inhibitor, the type of metal under study, the temperature and the surface activity [32]. The isotherm represents a mechanistic view of how the inhibitor under study interacts with this aggressive environment and the metal/alloy.
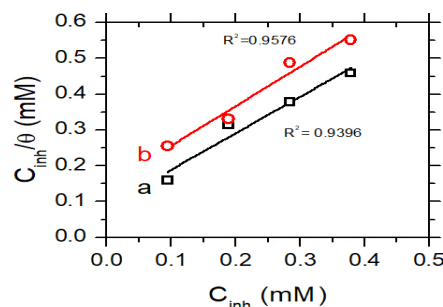
Fig. 13 Langmuir adsorption isotherm for **Ch** (a) and **ChN** inhibitors during acid cleaning of mild steel in 0.5M HCl.

There are many adsorption isotherms describing the relationship between the adsorbate and the metal surface, including for example Langmuir, Temkin, Freundlich, Frumkin and many others. The

Langmuir adsorption isotherm [28, 33-35] assumes the adsorbate forms a monolayer.

According to Eq. 14, the surface coverage in this isotherm is proportional to the adsorbate concentration, where C_{inh} is the inhibitor concentration in mol/L while θ is the degree of surface coverage, and K_{ads} is the adsorption-desorption equilibrium constant and α is the adsorbate interaction parameter. The K_{ads} can be calculated from the intersection of the data shown in Fig. 13.

$$K_{ads}C_{inh} = \frac{\theta}{1-\theta}(Langmuir) \quad (14)$$

K_{ads} was calculated using the surface coverage after 4 hours of immersion during the weight loss experiment. For the **Ch** inhibitor, the K_{ads} was calculated to be 11.4824 M^{-1}, while for the **ChN** sample, the K_{ads} reached 6.8667 M^{-1}.

The data showed that the Ni complex (**Ch**) adsorption-desorption equilibrium constant was higher than that for the **ChN** inhibitor implying that the **ChN** was not uniformly distributed on the MS surface during its immersion in the 0.5M HCl.

From the calculated K_{ads} values, the standard free energy of adsorption (ΔG^o_{ads}) can be calculated by the following relationship:

$$K_{ads} = \frac{1}{55.5}\exp\left(-\frac{\Delta G^o_{ads}}{RT}\right) \quad (15)$$

where 55.5 is the molar water concentration in the solution expressed in M (mol/L^{-1}), R is the universal gas constant (8.314 J K^{-1} mol^{-1}) and T is the absolute temperature (K).

The ΔG^o_{ads} for the **Ch** inhibitor was calculated to be -12.1685 kJ mol^{-1} while for the **ChN** inhibitor, it was calculated to be -14.7326 kJ mol^{-1}.

The negative sign of both inhibitors indicated that they were spontaneously adsorbed on the metal surface in 0.5M HCl. In general, the value of ΔG^o_{ads} is used to determine the nature of the adsorption process; when ΔG^o_{ads} is less negative than 20 kJ mol^{-1}, the interaction of the inhibitor molecules with the metal surface is primarily physical, whereas if ΔG^o_{ads} is more negative than 40 kJ mol^{-1}, charge sharing from the inhibitor to the metal can cause chemisorption. Both physical and chemical adsorptive interactions can be assumed when ΔG^o_{ads} is between -20 and -40 kJ mol^{-1}. As a result of data obtained in this study, the **Ch** and **ChN** inhibitors were physically adsorbed on the surface of MS.

3.3.4. Raman Spectroscopy

Figure 14 shows the Raman spectroscopy of the surface of the MS after immersion alone and after addition of **Ch** and **ChN** inhibitors in 0.5M HCl at 30°C
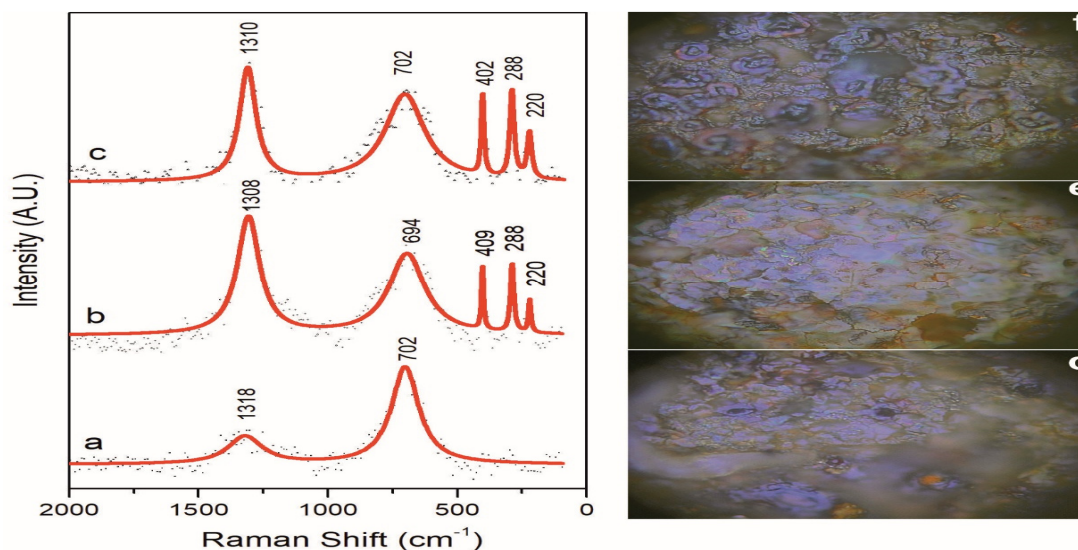
Fig. 14 Raman spectroscopy of mild steel surface (a), MS after the addition of **Ch** inhibitor (b) and MS after the addition of **ChN** inhibitor (c). The optical microscope images at 100 X magnification for MS (d), MS after the addition of **Ch** inhibitor (e) and MS after the addition of **ChN** inhibitor (f). All samples immersed in 0.5M HCl at 30°C for 4 hr prior to investigation and inhibitor concentration was 100 ppm.

for 5 hours. The Raman spectra after addition of the **Ch** and **ChN** inhibitors were almost identical.

The Raman analysis CCD images revealed orange-colored deep pits on the surface of the MS sample after 4 hours of immersion in 0.5M HCl. However, after the addition of the inhibitors, the pits were covered with a layer of an organic material, which was more effective in the case of the **ChN** inhibitor than in the case of the **Ch** inhibitor in reducing the exposed pits on the surface of MS to HCl exposure. Raman spectroscopy reveals no discernible difference between the two spectra.

After immersing a coupon of MS in 0.5M HCl for 4 hours without the addition of any inhibitors, Raman spectroscopy was able to identify iron oxyhydroxide (FeOOH) at 702 cm^{-1}, and the other peak at 1318 cm^{-1} which was characteristic of FeOOH (lepidocrocite) as outer layer corrosion product, indicating that the FeOOH was in gamma form [36]. The peak formed at 702 cm^{-1} was compared to that reported early by Criado et al [37].After immersing the coupon of MS in 0.5M HCl for 4 hours and introducing 100 ppm of either **Ch** inhibitor or **ChN** inhibitors to this system, Raman spectra shows additional three peaks at approximately 409, 288, and 220 cm^{-1} and the original peak appeared

$$Fe^{2+} + 2OH^- \longrightarrow Fe(OH)_2 \qquad (18)$$

$$2Fe(OH)_2 + O_2 + H_2O \longrightarrow 2Fe(OH)_3 \qquad (19)$$

$$Fe(OH)_3 \longrightarrow FeOOH + H_2O \qquad (20)$$

$$4Fe + 3O_2 + 2H_2O \longrightarrow 4FeOOH \qquad (21)$$

$$Fe^{2+} + 2Cl^- \longrightarrow FeCl_2 \qquad (22)$$

$$Fe^{3+} + 3Cl^- \longrightarrow FeCl_3 \qquad (23)$$

$$FeCl_2 + 2H_2O \longrightarrow Fe(OH)_2 + 2HCl \qquad (24)$$

$$FeCl_3 + 3H_2O \longrightarrow Fe(OH)_3 + 3HCl \qquad (25)$$

$$8FeOOH + Fe^{2+} + 2e^- \longrightarrow 3Fe_3O_4 + 4H_2O \quad (26)$$
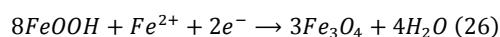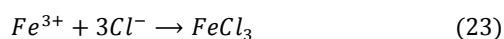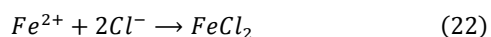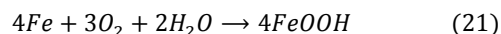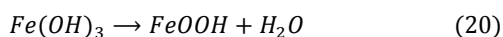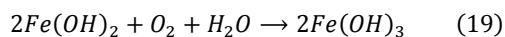
at 1318 cm^{-1} shifted slightly to 1308 and 1310 cm^{-1} for the **Ch** and **ChN** inhibitors respectively. The original γ-FeOOH peaks were still preserved.

The peak at 409 cm^{-1} may be attributed to the NH wag region or NH$_2$ sym stretching [37], whereas the peak at 288 cm^{-1} is attributed to the benzene ring as previously calculated [37]. The peak at 220 cm^{-1} matched the peak at 215 cm^{-1} [37], attributed to the formation of modified hematite where this phase is considered to be the most thermodynamically stable iron oxide phase under ambient conditions. In comparison to this work, their

detection to this phase was at a lower laser power of around 5 mW. In this study, it appears that the presence of both inhibitors added to the 0.5M HCl accelerated hematite formation.

The formation of γ-FeOOH (lepidocrocite) was explained by the reaction of iron with Cl$^-$ to form iron(I) chloride, which on hydrolysis formed γ-FeOOH, as the sole corrosion product formed under the conditions described above. Lepidocrocite was reported to be an unstable and non-protective oxide [38].

It is worth to mention herein that the laser excitation and the laser beam power may affect the quality of results of the analysis where at high power laser may resulted in the oxidation of the corrosion products on the surface of the base metal [39, 40]

Cathodic reaction represented by Eq (16) while anodic reaction represented by Eq (17)

$$O_2 + 2H_2O + 4e^- \longrightarrow 4OH^- \qquad (16)$$

$$Fe \longrightarrow Fe^{2+} + 2e^- \qquad (17)$$
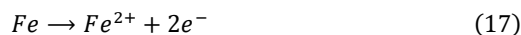
The formation of FeOOH can be discussed in two ways. The first is to use the OH anions produced by the cathodic reaction, as shown in Eq 16, and the iron cations produced by the anodic reaction, as shown in Eq 17. The second way is to use the Cl anions from the HCl and the iron cations from the anodic reaction (Eq. 17).

Dehydrating the iron(III) hydroxide as described in Eq. 20 produced the FeOOH, and similarly, the Fe(OH)$_3$ produced in Eq. 28 dehydrated to produce the FeOOH, which Raman spectroscopy confirmed as lepidocrocite.

The lack of detection of the magnetite passive film (Eq. 26) by Raman spectroscopy could be attributed to the relatively short time we used during the acid cleaning process or the relatively low concentration of HCl used in this work. Instead, a hematite phase was detected which was possibly formed due to the presence of the inhibitors which catalyse its formation in the HCl acid solution.

Conclusions

The synthesized novel Ni complex of isonicotinohydrazide from chalcone elucidated by spectral analysis, showed inhibition efficiency for MS during acid cleaning in 0.5M HCl. This inhibition was confirmed by computational analysis using the DFT/B3PW91/LANL2DZ basis set and showed

excellent compatibility between the Ni complex and the ligand (chalocone).

- The experimental corrosion techniques demonstrate that the corrosion of MS during the 0.5M HCl acid wash was suppressed by **Ch** and **ChN** (Chalcone and its nickel complex, respectively).

- According to weight loss data, the **ChN** inhibitor's maximum value was 73.5, while the **Ch** inhibitor's greatest value was 82.4%.

- The OCP exhibits a shift in the noble direction when compared to the control proving as preliminary evidence of the success of these two compounds studied.

- Results from PDP indicated that the **Ch** inhibitor had an inhibitory efficacy of ~86.9% and the **ChN** inhibitor of ~92.3% which support the OCP results.

- The difference between WL and PDP results is that the WL technique had a longer immersion of the MS coupons in 0.5M HCl compared to the PDP technique. This time increase led to an increase in HCl concentration and consequently affected the results in the WL technique.

- When a maximum concentration of 100 ppm was reached for PDP, the polarization resistance for the **ChN** inhibitor was higher than that for the **Ch** inhibitor, and a concomitant decrease in the corrosion rate with increasing **ChN** inhibitor concentration was observed.

- Because of their high inhibition efficiency at such low concentrations studied, the new compounds are promising.

Conflicts of interest

All authors confirm that there are no conflicts to declare.

References

[1] L. Fragoza-Mar, O. Olivares-Xometl, M.A. Dominguez-Aguilar, E.A. Flores, P. Arellanes-Lozada, F. Jimenez-Cruz, Corrosion inhibitor activity of 1,3-diketone malonates for mild steel in aqueous hydrochloric acid solution, Corrosion Sci. 61 (2012) 171-184.

[2] I. Elazhary, A. Boutouil, H.B. El Ayouchia, M.R. Laamari, M. El Haddad, H. Anane, S.-E. Stiriba, Anti-corrosive properties of (1-benzyl-1H-1, 2, 3-triazol-4-yl) methanol on mild steel corrosion in hydrochloric acid solution: experimental and theoretical evidences, Prot. Met. Phys. Chem. Surf. 55(1) (2019) 166-178.

[3] M. Filali, E. El Hadrami, A. Bentama, B. Hafez, I. Abdel-Rahman, A. Harrach, H. Elmsellem, B. Hammouti, M. Mokhtari, S. Stiriba, 3, 6-Di (pyridin-2-yl) pyridazine derivatives as original and new corrosion inhibitors in support of mild steel: Experimental studies and DFT investigational, Int. J. Corros. Scale Inhib., 2019, pp. 93-109.

[4] G.I. Youssef, A.E. El Meleigy, L.A. Khorshed, A. Attia, E.A. Ashour, Inhibitive effect of benzotriazole on the corrosion and corrosion fatigue of α-Al bronze alloy in LiBr solution, Materials and Corrosion 69(12) (2018) 1827-1836.

[5] A. Attia, H.T. Abdel-Fatah, Triton X-100 as a Non-Ionic Surfactant for Corrosion Inhibition of Mild Steel During Acid Cleaning, Met. Mater.-Int. (2019) 1-10.

[6] F.S. Cui, Y.Q. Ni, J.C. Jiang, L. Ni, Z.R. Wang, Experimental and theoretical studies of five imidazolium-based ionic liquids as corrosion inhibitors for mild steel in H2S and HCl solutions, Chem. Eng. Commun. (2020) 14.

[7] A. Attia, L. Khorshed, S. Morsi, E. Ashour, Corrosion protection of some Cu-based alloys by polyacrylate-alumina nanocomposite coatings, Anti-Corros. Methods Mater. (2021).

[8] S.M. Siddiqui, A. Salahuddin, A. Azam, Synthesis, characterization and antiamoebic activity of some hydrazone and azole derivatives bearing pyridyl moiety as a promising heterocyclic scaffold, European journal of medicinal chemistry 49 (2012) 411-416.

[9] A. Boutouil, I. Elazhary, M.R. Laamari, H. Ben El Ayouchia, H. Anane, M. El Haddad, S.E. Stiriba, An exploration of corrosion inhibition of mild steel in sulphuric acid solution through experimental study and Monte Carlo simulations, J. Adhes. Sci. Technol. 34(5) (2020) 549-578.

[10] D. Seifzadeh, V. Valizadeh-Pashabeigh, A. Bezaatpour, 5-CM-Salophen Schiff base as an effective inhibitor for corrosion of mild steel in 0.5 M HCl, Chem. Eng. Commun. 203(10) (2016) 1279-1287.

[11] A. Toghan, H. Gadow, H.M. Dardeer, H. Elabbasy, New promising halogenated cyclic imides derivatives as potential corrosion inhibitors for carbon steel in hydrochloric acid solution, J. Mol. Liq. 325 (2021) 115136.

[12] I.B. Obot, A. Madhankumar, S.A. Umoren, Z.M. Gasem, Surface protection of mild steel using benzimidazole derivatives: experimental and theoretical approach, J. Adhes. Sci. Technol. 29(19) (2015) 2130-2152.

[13] B.H. Stuart, Infrared spectroscopy: fundamentals and applications, John Wiley & Sons2004.

[14] A.M. Fahim, H.S. Magar, M.A. Ayoub, Synthesis, characterization, thermal studies, electrochemical behavior, antimicrobial, docking studies, and computational simulation of triazole-thiol metal complexes, Applied Organometallic Chemistry 36(5) (2022) e6647.

[15] A.M. Fahim, H.S. Magar, N.H. Mahmoud, Synthesis, anti-proliferative activities, docking studies, and computational calculations of novel isonicotinic mixed complexes, Applied Organometallic Chemistry 36(5) (2022) e6616.

[16] N.H. Mahmoud, G.H. Elsayed, A. Aboelnaga, A.M. Fahim, Spectroscopic studies, DFT calculations, cytotoxicity activity, and docking stimulation of novel metal complexes of Schiff base ligand of isonicotinohydrazide derivative, Applied Organometallic Chemistry (2022) e6697.

[17] N.H. Mahmoud, A.A. Emara, W. Linert, A.M. Fahim, A. Abou-Hussein, Synthesis, spectral investigation, biological activities and docking stimulation of novel metal complexes of Trifluoro phenylthiazol derivative with computational studies, J. Mol. Struct. 1272 (2023) 134095.

[18] S. Kaya, P. Banerjee, S.K. Saha, B. Tüzün, C. Kaya, Theoretical evaluation of some benzotriazole and phospono derivatives as aluminum corrosion inhibitors: DFT and molecular dynamics simulation approaches, RSC Adv. 6(78) (2016) 74550-74559.

[19] J. Hinze, H.H. Jaffe, Electronegativity. I. Orbital electronegativity of neutral atoms, Journal of the American Chemical Society 84(4) (1962) 540-546.

[20] I.B. Obot, D.D. Macdonald, Z.M. Gasem, Density functional theory (DFT) as a powerful tool for designing new organic corrosion inhibitors. Part 1: An overview, Corrosion Sci. 99 (2015) 1-30.

[21] P. Geerlings, F. De Proft, W. Langenaeker, Conceptual density functional theory, Chemical reviews 103(5) (2003) 1793-1874.

[22] M. Stern, A. Geary, A theoretical analysis of the shape of polarization curves, J. Electrochem. Soc 104(1) (1957) 56-63.

[23] Z.T. Khudhair, M.S. Shihab, Study of Synergistic Effect of Some Pyrazole Derivatives as Corrosion Inhibitors for Mild Steel in 1 M H2SO4, Surf. Eng. Appl. Electrochem. 56(5) (2020) 601-609.

[24] F.K. Ojo, I.A. Adejoro, J.A. Lori, O.E. Oyeneyin, K.G. Akpomie, Indole Derivatives as Organic Corrosion Inhibitors of Low Carbon Steel in HCl Medium-Experimental and Theoretical Approach, Chem. Afr. J. Tunisian Chem. Soc. (2022) 14.

[25] D.K. Singh, E.E. Ebenso, M.K. Singh, D. Behera, G. Udayabhanu, R.P. John, Non-toxic Schiff bases as efficient corrosion inhibitors for mild steel in 1 M HCl: Electrochemical, AFM, FE-SEM and theoretical studies, J. Mol. Liq. 250 (2018) 88-99.

[26] Y. Boughoues, M. Benamira, M. Lyamine, N. Bouider, S. Abdelaziz, Experimental and theoretical investigations of four amine derivatives as effective corrosion inhibitors for mild steel in HCl medium, RSC Adv. 10(40) (2020) 24145-24158.

[27] A. Yasir, A. Khalaf, M. Khalaf, Preparation, characterization, evaluation of polymeric resin (BHMET) from the reaction of malic anhydride with recycled PET as a corrosion inhibitor for C-steel in HCl, Rev. Innovaciencia 7(1) (2019) 11.

[28] A. Pradityana, Sulistijono, A. Shahab, L. Noerochim, D. Susanti, Inhibition of Corrosion of Carbon Steel in 3.5% NaCl Solution by Myrmecodia Pendans Extract, Int. J. Corros. 2016 (2016) 6.

_____

[29] A.I. Obike, P.C. Okafor, K.J. Uwakwe, X. Jiang, D. Qu, The inhibition of CO2 corrosion of L360 mild steel in 3.5% NaCl solution by imidazoline derivatives, Int. J. Corros. Scale Inhib. 7(3) (2018) 318-330.

[30] S. Mammeri, N. Chafai, H. Harkat, R. Kerkour, S. Chafaa, Protection of Steel Against Corrosion in Acid Medium Using Dihydropyrimidinone Derivatives: Experimental and DFT Study, Iran. J. Sci. Technol. Trans. A-Sci. (2021) 13.

[31] B.N. Abba, R. Idouhli, A.T. Ilagouma, A. Abouelfida, M. Khadiri, A. Romane, Use of Endostemon tereticaulis (Pear.) M.Ashby and Hyptis spicigera Lam. Plant Extracts as Corrosion Green Inhibitors for Mild Steel in 1M HCl: Electrochemical and Surface Morphological Studies, Prot. Met. Phys. Chem. Surf. 57(3) (2021) 619-633.

[32] A.A. El-Awady, B.A. Abd-El-Nabey, S.G. Aziz, Kinetic-thermodynamic and adsorption isotherms analyses for the inhibition of the acid corrosion of steel by cyclic and open-chain amines, J. Electrochem. Soc. 139(8) (1992) 2149.

[33] A. Benabida, N. El-Aouni, M. Galai, A. El Assyry, O. Dagdag, M. Cherkaoui, A. El Harfi, A. Zarrouk, The New Organic Molecule-Based Epoxy Resin as an Effective Corrosion Inhibitor for Mild Steel in Sulfuric Acid Medium, Prot. Met. Phys. Chem. Surf. 57(1) (2021) 199-210.

[34] A. Tazouti, N. Errahmany, M. Rbaa, M. Galai, Z. Rouifi, R. Touir, A. Zarrouk, S. Kaya, M.E. Touhami, B. El Ibrahimi, Effect of hydrocarbon chain length for acid corrosion inhibition of mild steel by three 8-(n-bromo-R-alkoxy) quinoline derivatives: experimental and theoretical investigations, J. Mol. Struct. 1244 (2021) 130976.

[35] L.M. Vračar, D.M. Dražić, Adsorption and corrosion inhibitive properties of some organic molecules on iron electrode in sulfuric acid, Corrosion Sci. 44(8) (2002) 1669-1680.

[36] I.A. Kartsonakis, C.A. Charitidis, Corrosion Protection Evaluation of Mild Steel: The Role of Hybrid Materials Loaded with Inhibitors, Appl. Sci.-Basel 10(18) (2020) 18.

[37] M. Criado, S. Martínez-Ramirez, J.M. Bastidas, A Raman spectroscopy study of steel corrosion products in activated fly ash mortar containing chlorides, Constr. Build. Mater. 96 (2015) 383-390.

[38] R.M. Cornell, U. Schwertmann, The iron oxides: structure, properties, reactions, occurrences, and uses, Wiley-vch Weinheim2003.

[39] J. Singh, D. Singh, The nature of rusts and corrosion characteristics of low alloy and plain carbon steels in three kinds of concrete pore solution with salinity and different pH, Corrosion Sci. 56 (2012) 129-142.

[40] R.J. Thibeau, C.W. Brown, R.H. Heidersbach, Raman spectra of possible corrosion products of iron, Applied spectroscopy 32(6) (1978) 532-535.

_____